2024-01-02

Mathematical modeling of vehicle carbon dioxide emissions

Mayengo, Maranya

Cell Press

Heliyon 10 (2024) e23976

Contents lists available at ScienceDirect

Heliyon

journal homepage: www.cell.com/heliyon

Research article

Mathematical modeling of vehicle carbon dioxide emissions

Pita Donald [a,b,*], Maranya Mayengo [a], Aristide G. Lambura [c]

[a] School of Computational and Communication Science and Engineering, Nelson Mandela African Institution of Science and Technology (NM-AIST), P.O. Box 447, Arusha, Tanzania

[b] Department of Mathematics, Humanities and Social Sciences, National Institute of Transport (NIT), P.O. Box 7O5, Dar es Salaam, Tanzania

[c] Department of Computer Systems and Mathematics, Ardhi University (ARU), P.O. Box 35176, Dar es Salaam, Tanzania

ARTICLE INFO

Keywords:
Mathematical model
Vehicular emission
Greenhouse gas
Atmospheric carbon dioxide
Climate change
Sustainable transportation

ABSTRACT

The demand for transportation, driven by an increasing global population, is continuously rising. This has led to a higher number of vehicles on the road and an increased reliance on fossil fuels. Consequently, the rise in atmospheric carbon dioxide (CO_2) levels has contributed to global warming. Therefore, it is important to consider sustainable transportation practices to meet climate change mitigation targets. In this research paper, a non-linear mathematical model is developed to study the dynamics of atmospheric CO_2 concentration in relation to human population, economic activities, forest biomass, and vehicle population. The developed model is analyzed qualitatively to understand the long-term behavior of the system's dynamics. Model parameters are fitted to actual data of world population, human economic activities, atmospheric CO_2, forest biomass, and vehicle population. It is shown that increased vehicular CO_2 emissions have a potential contribution to the increase in atmospheric CO_2 and the decline of human population. Numerical simulations are carried out to verify the analytical findings and we performed global sensitivity analysis to explore the impacts of different sensitive parameters on the CO_2 dynamics.

1. Introduction

Greenhouse gases, with carbon dioxide (CO_2) being a prominent example, play a significant role in the greenhouse effect, a key driver of climate change. These gases are emitted by diverse economic sectors, including energy generation, industrial processes, building operations, transportation activities, agricultural practices, forestry, and other land use activities (AFOLU). The expanding global population and corresponding economic development have led to an increased demand for energy, primarily sourced from fossil fuels [1–4]. This heightened energy demand has resulted in higher carbon dioxide (CO_2) emissions, exacerbating the challenges posed by climate change [5–7].

The transportation sector is a significant contributor to CO_2 emissions due to the combustion of fossil fuels, which contributes to the concentration of atmospheric CO_2 [8–11]. Urban transport alone accounted for 23% of total energy-related emissions, and the global transportation sector contributes approximately 25% of total CO_2 emissions from fossil fuel combustion [10,12]. Consequently, climate-related issues such as ozone layer depletion, droughts, and global warming have become more pronounced.

* Corresponding author at: School of Computational and Communication Science and Engineering, Nelson Mandela African Institution of Science and Technology (NM-AIST), P.O. Box 447, Arusha, Tanzania.
E-mail address: donaldp@nm-aist.ac.tz (P. Donald).

https://doi.org/10.1016/j.heliyon.2024.e23976
Received 18 June 2023; Received in revised form 21 November 2023; Accepted 2 January 2024

Available online 8 January 2024

Table 1
Model parameters and description.

Parameter	Description
r	Intrinsic human population growth rate
L	Human population carrying capacity
α	Mortality rate coefficient due to enhanced CO_2
s	Economic activities growth rate due to population
τ	Human economic activities growth rate due to vehicle population
η	Human economic activities depletion rate constant
C_0	Emission rate of CO_2 from natural and respiration processes
γ	CO_2 vehicle emission rate constant
σ	Human economic activities CO_2 emission rate
ρ	CO_2 depletion rate coefficient due to forest biomass
π	Natural CO_2 depletion rate coefficient
θ	Forest biomass intrinsic growth rate coefficient
K	Forest area carrying capacity
ψ	Deforestation rate coefficient
β	Vehicle's population growth rate due to demand for mobility
ξ	Vehicle depletion rate coefficient
ω	Human population growth rate coefficient due forest harvesting

At the forefront of contemporary discourse, complexity sciences play a pivotal role in preserving human lives. This discourse encompasses the strategic application of mathematical modeling as a potent instrument within this paradigm [13]. Recent studies have employed non-linear mathematical models to investigate the dynamics of atmospheric CO_2 in relation to forest biomass. Notably, [14–16] have explored these models. These investigations have delved into diverse strategies, including genetically engineered plants and incentives for energy conservation through education, aimed at curtailing CO_2 emissions. Additionally, [17] has contributed to the discourse by scrutinizing the dynamics of atmospheric CO_2 from an energy sector perspective, highlighting the significance of adopting low-carbon energy sources to mitigate costs. Furthermore, [18,19] have employed non-linear mathematical models to manage atmospheric CO_2 levels through reforestation, considering variables such as forest biomass, human population, and reforestation efforts. Likewise, [15] have utilized a non-linear mathematical model to study atmospheric CO_2 concentration, taking into account plants' capacity to absorb atmospheric CO_2.

However, non of these studies considered the dynamics of atmospheric CO_2 concentration due to vehicle emissions. Therefore, this study comes up with a mathematical model that encompasses the interplay or dynamics between human population, human economic activities, forest biomass, vehicle population and atmospheric CO_2 concentration in a global scale, and investigate the impact of vehicle population on the dynamics of atmospheric CO_2 concentration and human population. The structure of this paper is well-organized, with sections dedicated to formulating the mathematical model, qualitative analysis, quantitative analysis, and concluding the findings.

2. Model formulation

The system of non-linear ordinary differential equations is used to describe the dynamics of atmospheric CO_2 concentration. The model is made up of five distinct compartments, namely, human population (N), human economic activities (H), atmospheric CO_2 concentration (C), forest biomass (B) and vehicle population (V) at a time t. It is assumed that the human population grows logistically and depletes due to the adverse impact of increased atmospheric CO_2 concentration by a rate α [14,20]. Also, it is assumed that human population increases due to consumption of forest resources by a rate ω [14]. Using these assumptions, the dynamics of human population is governed by the equation (1) and parameter descriptions are in Table 1

$$\dot{N} = rN\left(1 - \frac{N}{L}\right) + \omega\psi NB - \alpha CN \tag{1}$$

Human economic activities are assumed to expand in response to population growth, as it drives increased demand for goods and services, and depletes naturally by a rate η. The growth of human activities is assumed to be influenced by the number of vehicles by the rate τ. As number of vehicle increases, it stimulates various economic sectors and promotes overall economic growth. This, in turn, leads to an expansion of human activities and their impact on the environment. Additionally, we assume that the growth of human economic activities is quantified by the Gross Domestic Product (GDP). The GDP serves as an indicator of economic performance and reflects the overall value of goods and services produced within a country. As GDP increases, it signifies a higher level of economic activity, including industrial, commercial, and agricultural sectors. The dynamics of human economic activities can be modeled by the equation (2) and its parameters are detailed in Table 1.

$$\dot{H} = sN + \tau V - \eta H \tag{2}$$

The atmospheric CO_2 concentration is assumed to increase due to the growing number of vehicles and human activities by rates γ and σ respectively. Additionally, CO_2 concentration in the atmosphere is naturally depleted through ocean sinking and absorbed by forest through photosynthesis process [21,4]. The growth rate of atmospheric CO_2 resulting from natural processes, such as

respiration of living organisms, volcanic eruptions, and changes in ocean circulation, is assumed to be constant [18]. The dynamics of atmospheric CO_2 is governed by equation (3) and parameters are described in a Table 1.

$$\dot{C} = C_0 + \gamma V + \sigma H - \rho BC - \pi C \tag{3}$$

It is presumed that forest biomass adheres to the principles of logistic growth and depletes due to human population growth. Its dynamics is governed by equation (4) and parameters are explained in a Table 1.

$$\dot{B} = \theta B\left(1 - \frac{B}{K}\right) - \psi N B \tag{4}$$

In the region of consideration, the vehicle population is assumed to have a growth rate of β and naturally depletes, by the rate ξ. Vehicle population dynamics is modeled by equation (5).

$$\dot{V} = \beta N - \xi V \tag{5}$$

Consequently, we formulate the following system of equations of non linear differential equation as presented in a system (6).

$$\begin{cases} \dot{N} = rN\left(1 - \frac{N}{L}\right) + \omega\psi N B - \alpha C N \\ \dot{H} = sN + \tau V - \eta H \\ \dot{C} = C_0 + \gamma V + \sigma H - \rho BC - \pi C \\ \dot{B} = \theta B\left(1 - \frac{B}{K}\right) - \psi N B \\ \dot{V} = \beta N - \xi V \end{cases} \tag{6}$$

Where

$$N(0) \geq 0, H(0) \geq 0, C(0) > 0, B(0) \geq 0, V(0) \geq 0 \tag{7}$$

3. Qualitative analysis

3.1. Boundedness of model solution

In this section, we demonstrate that the solutions of a system (6) with the initial condition (7) remain bounded. We achieve this by employing a well-established comparison theorem for differential equations [22]. In Lemma (1), we determine the region of attraction, which is an invariant region attracting all solutions of the model system (6) with the initial condition (7).

Lemma 1. *The set* $\Omega = \{(N, H, C, B, V) \in \mathbb{R}^5 : 0 \leq N \leq N_m; 0 \leq H \leq H_m; 0 < C \leq C_m; 0 \leq B \leq B_m;\ 0 \leq V \leq V_m$, *where* $N_m = L + \frac{\omega\psi KL}{r}$, $H_m = \frac{sN_m}{\eta}$, $C_m = \frac{\eta C_0 + s\sigma N_m}{\eta(\rho K + \pi)}$, $B_m = K$, $V_m = \frac{\beta N_m}{\xi}$ *establish the region of attraction for the system (6), which attracts all solutions originating from within the positive orthant's interior.*

Proof for Lemma (1) is appended in Appendix B.

3.2. Equilibrium analysis

The long-term behavior of the system (6) was established by using stability theory. The feasible equilibrium points are obtained and their stability properties are established. The model system (6) has two non-negative trivial solutions $E_1\left(0, 0, \frac{C_0}{\pi}, 0, 0\right)$ and $E_2\left(0, 0, \frac{\theta C_0}{K\rho + \pi}, K, 0\right)$ and two non-trivial solutions $E_3\left(N_3, H_3, C_3, 0, V_3\right)$ and $E^*(N^*, H^*, C^*, B^*, V^*)$.

It can be noted that the existence of E_1 and E_2 is obvious. Further more the existence of equilibria E_3 and E^* depend on the satisfaction of condition (8).

$$\frac{r}{\alpha} - \frac{C_0}{\pi} > 0 \tag{8}$$

Existence of E_3

To prove the existence of E_3 we solved the system (9) to obtain algebraic equations for N_3, H_3, C_3 and V_3 [17]. Consider the system (9) below,

$$\left.\begin{aligned} r\left(1-\frac{N_3}{L}\right)-\alpha C_3 &= 0\\ sN_3+\tau V_3-\eta H_3 &= 0\\ C_0+\gamma V_3+\sigma H_3-\pi C_3 &= 0\\ \beta N_3-\xi V_3 &= 0 \end{aligned}\right\}. \tag{9}$$

From system (9) we have the following equations

$$V_3=\frac{\beta N_3}{\xi}. \tag{10}$$

$$C_3=\frac{\eta\xi C_0+(\gamma\beta\eta+\sigma(s\xi+\tau\beta))N_3}{\pi\xi\eta}=f(N_3). \tag{11}$$

$$H_3=\frac{s\xi N_3+\tau\beta N_3}{\eta\xi}. \tag{12}$$

On the other hand, the first equation provides $g(N_3)$ such that

$$g(N_3)=r\left(1-\frac{N_3}{L}\right)-\alpha f(N_3). \tag{13}$$

By using equation (13), we analyze $g(N_3)$ in three different scenarios as follows:

(a) When $N_3=L+\dfrac{\omega\psi KL}{r}$ we have the following

$$-\left(\omega\psi KL+\frac{\eta\xi C_0 r+(\gamma\beta\eta+\sigma(s\xi+\tau\beta))(rL+\omega\psi KL)}{\pi r\xi\eta}\right)<0.$$

(b) At $N_3=0$, a function $g(N_3)$ is given by

$$g(0)=\alpha\left(\frac{r}{\alpha}-\frac{C_0}{\pi}\right).$$

Since $g\left(L+\dfrac{\omega\psi KL}{r}\right)<0$, there exist a positive root N_3 in the interval of $0<N_3<L+\dfrac{\omega\psi KL}{r}$ if and only if $g(0)>0$. Clearly, this requirement is met upon satisfaction of condition (8).

(c) For uniqueness of $N=N_3$, we need to prove that $g'(N_3)<0$. Considering equation (13) and some algebraic simplifications, it can be easily shown that

$$g'(N_3)=-\left(\frac{r}{L}+\alpha\frac{\gamma\beta\eta+\sigma(s\xi+\tau\beta)}{\pi\xi\eta}\right)<0.$$

Thus, a unique positive root, say $N=N_3$ of the equation (13) lies on interval $0<N_3<L+\dfrac{\omega\psi KL}{r}$. Substituting $N=N_3$ into equations (10)–(12) we get the appropriate values of $V=V_3$, $C=C_3$ and $H=H_3$. Hence, it can be concluded that an equilibrium point E_3 exists, whenever the condition (8) holds.

Existence of E^*

Interior equilibrium point E^* of the system (6) can be obtained by solving the system (14).

$$\left.\begin{aligned} r\left(1-\frac{N^*}{L}\right)-\alpha C^*+\omega\psi B^* &= 0\\ sN^*+\tau V^*-\eta H^* &= 0\\ C_0+\gamma V^*+\sigma H^*-\rho B^*C^*-\pi C^* &= 0\\ \theta\left(1-\frac{B^*}{K}\right)-\psi N^* &= 0\\ \beta N^*-\xi V^* &= 0 \end{aligned}\right\} \tag{14}$$

The solution of the system (14) establishes the following results

$$V^*=\frac{\beta N^*}{\xi} \tag{15}$$

$$H^*=\frac{(s\xi+\tau\beta)N^*}{\xi\eta} \tag{16}$$

$$B^*=\frac{K}{\theta}\left(\theta-\psi N^*\right) \tag{17}$$

$$C^* = \frac{\eta C_0 \xi + \eta\gamma\beta N^* + \sigma N^*(s\xi + \tau\beta)}{\eta\xi(\rho B^* + \pi)} \tag{18}$$

$$h(N^*, B^*) = r\left(1 - \frac{N^*}{L}\right) - \frac{\alpha}{\eta\xi\pi}\left(\xi\eta C_0 + \xi\gamma\beta N^* + \sigma N^*(s\xi + \tau\beta)\right) + \omega\psi B^* \tag{19}$$

From equation (19) when no forest resources ($B^* = 0$) we get the following function of N^*

$$f(N^*) = r\left(1 - \frac{N^*}{L}\right) - \frac{\alpha}{\eta\xi\pi}\left(\xi\eta C_0 + \xi\gamma\beta N^* + \sigma N^*(s\xi + \tau\beta)\right). \tag{20}$$

By using equation (20) $f(N^*)$ can be analyzed as follows,

(a) We evaluate a function $f(N^*)$ at $N^* = 0$ to get the following

$$f(0) = \alpha\left(\frac{r}{\alpha} - \frac{C_0}{\pi}\right) > 0$$

(b) When $N^* = L + \dfrac{\omega\psi KL}{r}$ we have the following

$$-\left[\omega\psi K + \frac{\alpha}{\eta\xi\pi r}\left[r\xi\eta C_0 + (rL + \omega\psi KL)(\xi\gamma\beta + (s\xi + \tau\beta)\sigma)\right]\right] < 0$$

There exists a positive root $N = N^*$ of equation (20) in the interval $(0, L + \dfrac{\omega\psi KL}{r})$ under condition (8).

(c) For uniqueness of $N = N^*$, we need $f'(N^*) < 0$, that is

$$f'(N^*) = -\left(\frac{r}{L} + \frac{\alpha}{\eta\xi\pi}(\xi\gamma\beta + \sigma(s\xi + \tau\beta))\right) < 0$$

Thus, a unique positive root, say N^* of the equation (20) lies on interval $0 < N^* < L + \dfrac{\omega\psi KL}{r}$. Substituting the obtained value of N^* into equations (15), (16) and (17) and performing algebraic simplifications we get the appropriate values of V^*, B^* and H^*. Since the values of N^* and B^* are known, then to obtain the value of C^* we substitute N^* and B^* into equation (18) and we conclude that an interior point E^* exists under condition (8).

3.3. Stability analysis

In this section the behaviors of different equilibrium points of the model system are analyzed. From the system (6) the Jacobian matrix is given by

$$J = \begin{pmatrix} r\left(1 - \frac{N}{L}\right) - \frac{rN}{L} - \alpha C + \omega\psi B & 0 & -\alpha N & \omega\xi N & 0 \\ s & -\eta & 0 & 0 & \tau \\ 0 & \sigma & -\rho B - \pi & -\rho C & \gamma \\ -\psi B & 0 & 0 & \theta\left(1 - \frac{B}{K}\right) - \frac{\theta B}{K} - \psi N & 0 \\ \beta & 0 & 0 & 0 & -\xi \end{pmatrix}.$$

At the equilibrium point $E_1\left(0, 0, \dfrac{C_0}{\pi}, 0, 0\right)$ the corresponding Jacobian matrix J_{E_1}, resulted from evaluating matrix J through E_1 is given by

$$J_{E_1} = \begin{pmatrix} \alpha\left(\frac{r}{\alpha} - \frac{C_0}{\pi}\right) & 0 & 0 & 0 & 0 \\ s & -\eta & 0 & 0 & \tau \\ 0 & \sigma & -\pi & \frac{-\rho C_0}{\pi} & \gamma \\ 0 & 0 & 0 & \theta & 0 \\ \beta & 0 & 0 & 0 & -\xi \end{pmatrix}.$$

The eigenvalues of a matrix J_{E_1} are $\lambda_1 = -\xi$, $\lambda_2 = \theta$, $\lambda_3 = -\eta$, $\lambda_4 = -\pi$ and $\lambda_5 = \dfrac{r}{\alpha} - \dfrac{C_0}{\pi} > 0$. The equilibrium point E_1 is unstable since it have at least one positive eigenvalues, that is $\lambda_2 > 0$ and $\lambda_5 > 0$.

Similarly, evaluating matrix J at E_2, the following matrix is established.

$$J_{E_2}=\begin{pmatrix} \frac{K^2\omega\psi\rho+K\pi\psi\omega+Kr\rho+\pi r-\alpha C_0}{\rho K+\pi} & 0 & 0 & 0 & 0 \\ s & -\eta & 0 & 0 & \tau \\ 0 & \sigma & -K\rho-\pi & \frac{-C_0\rho}{\rho K+\pi} & \gamma \\ -\psi K & 0 & 0 & -\theta & 0 \\ \beta & 0 & 0 & 0 & -\xi \end{pmatrix}.$$

The eigenvalues of J_{E_2} are $\lambda_1=-\xi$, $\lambda_2=-\theta$, $\lambda_3=-\eta$, $\lambda_4=-(K\rho+\pi)$, and $\lambda_5=\frac{K^2\omega\psi\rho+K\pi\psi\omega+Kr\rho+\pi r-\alpha C_0}{\rho K+\pi}$. Clearly, upon utilizing condition (8), $\lambda_5>0$ making E_2 unstable.

At the equilibrium point E_3, we establish a matrix J_{E_3}, such that

$$J_{E_3}=\begin{pmatrix} -\frac{rN_3}{L} & 0 & -\alpha N_3 & \omega\psi N_3 & 0 \\ s & -\eta & 0 & 0 & \tau \\ 0 & \sigma & -\pi & -\rho C_3 & \gamma \\ 0 & 0 & 0 & -\left(\psi N_3-\theta\right) & 0 \\ \beta & 0 & 0 & 0 & -\xi \end{pmatrix}.$$

$$N_3>\frac{\theta}{\psi} \tag{21}$$

Upon satisfaction of condition (21) all the entries at the main diagonal will be negative, following [15], we utilize the Gershgorin's Theorem by columns of the matrix to deduce sufficient conditions for local stability of E_3. As such, E_3 is proved to be asymptotically stable upon satisfaction of conditions in equation (22).

$$\begin{cases} \frac{L}{r}(s+\beta)<N_3<\frac{\pi}{\alpha} \\ \sigma<\eta \\ \frac{\rho C_m+\theta}{\psi(\omega+1)}<N_3<\frac{\rho C_m-\theta}{\psi(\omega-1)} \\ \tau+\gamma<\xi \end{cases} \tag{22}$$

Where C_m is defined in Lemma 1

Theorem 2. *The equilibrium point E_3, if exists, is locally asymptotically stable if conditions (22) are satisfied.*

At the interior equilibrium point E^*, the Jacobian matrix J, was evaluated to get a matrix J_{E^*}, such that

$$J_{E^*}=\begin{pmatrix} -\frac{rN^*}{L} & 0 & -\alpha N^* & \omega\psi N^* & 0 \\ s & -\eta & 0 & 0 & \tau \\ 0 & \sigma & -\rho B^*-\pi & -\rho C^* & \gamma \\ -\psi B^* & 0 & 0 & -\frac{\theta B^*}{K} & 0 \\ \beta & 0 & 0 & 0 & -\xi \end{pmatrix}.$$

Clearly, all entries in the main diagonal of J_{E^*} are negative. Following [15], we use the Gershgorin's Theorem by columns of the matrix to deduce the local stability of E^*. As such, E^* is proved to be locally asymptotically stable upon satisfaction of the following set of conditions

$$\begin{cases} N^*>\max\left\{\frac{L}{r}(\beta-\psi K),\frac{L}{r}(\psi K-\beta)\right\} \\ \sigma<\eta \\ N^*<\frac{\rho K-\pi}{\alpha} \\ \frac{\rho C_m-\theta}{\omega\psi}<N^*<\frac{\theta+\rho C_m}{\omega\psi} \\ \tau+\gamma<\xi \end{cases} \tag{23}$$

Where C_m is defined in lemma (1).

Theorem 3. *The interior equilibrium point E^*, if exists, is locally asymptotically stable if conditions (23) are satisfied.*

Theorem 4. *The interior equilibrium point E^*, if exists, is globally asymptotically stable in Ω if conditions (24) are satisfied.*

$$\left.\begin{aligned} r &> \min\left\{\frac{81\beta^2 L\gamma^2}{16\xi^2(\rho K+\pi)}, \frac{9\sigma^2 s^2}{16\eta(\rho K+\pi)}\right\} \\ L &< \max\left\{\frac{4(\rho K+\pi)}{9\alpha^2}, \frac{4\xi^2 s^2}{81\tau^2\beta^2}\right\} \end{aligned}\right\} \tag{24}$$

The proof of theorem (4) is presented in Appendix A.

3.4. Ecological interpretation of stability analysis

Equilibrium points E_1 and E_2 represent different situations regarding the extinction of the human population and the presence or absence of forest biomass. The point E_1 signifies the extinction of forest biomass, while E_2 represents a situation where forest biomass exists. The absence of human population would lead to the cessation of human-related activities, resulting in a lack of stabilization in atmospheric CO_2 concentration. Only natural processes such as volcanic eruptions will contribute to CO_2 emissions, resulting in a natural depletion of atmospheric CO_2 concentration. However, the analysis reveals further that the forest will rapidly grow up to its carrying capacity, acting as a sink for CO_2 absorption. The atmospheric CO_2 concentration will solely depend on natural processes and will naturally deplete.

The equilibrium point E_3 illustrates a situation where forest biomass no longer exists. In such a scenario, the emitted CO_2 will undergo some degree of natural absorption, while the remaining portion will persist in the atmosphere. This state is achieved when the natural growth rate of the human population exceeds the mortality rate resulting from the natural release of CO_2.

The interior equilibrium point E^* takes into account the coexistence of human population, economic activities, atmospheric CO_2 concentration, forest area, and vehicle population. To achieve this balance, the natural growth rate of the human population needs to exceed the mortality rate caused by natural CO_2 emissions. Moreover, specific conditions for the global stability of E^* must be met to ensure the stability of the atmospheric CO_2 concentration. When these conditions are satisfied, the forest biomass can absorb the existing atmospheric CO_2, safeguarding the environment, while the remaining CO_2 gradually decreases. These interpretations emphasize how human actions and natural processes interact, highlighting the critical importance of maintaining the necessary conditions to uphold the stability of atmospheric CO_2 concentration and environmental well-being.

4. Quantitative analysis

4.1. Parameter estimation and model fitting

The parameter estimation process was done by adjusting the model parameters to best fit the time series data of world population [23], atmospheric CO_2 concentration [24–26], forest area [27], number of vehicles produced [28], and Gross Domestic Product (GDP) [29]. The specific values of the parameters were obtained through the least squares method, which minimizes the sum of squared differences between the model predictions and the actual data. We use a MATLAB in-built function *(fminsearch)* that implements unconstrained nonlinear minimization (Nelder-Mead) to get candidates that serve as local minimizers for the sum of squared residuals [30]. The selection of initial parameter values was guided by the fulfillment of conditions outlined in the qualitative analysis section. In addition to the data-driven parameter estimation, values of $L = 11$, $C_0 = 5$ and $K = 750000$ were obtained from [31], [18] and [32] respectively. For the intrinsic human population growth rate (r), data from [23] was considered, where a range of 0.02 to 0.03 per year is considered [31]. This range provides an estimate for the value of r that is consistent with the available data and existing literature. The initial time is set to 1994, and the starting values are $N(0) = 5.66315$ billion people, $H(0) = 2,787.67662$ billion US$, $C(0) = 358.96$ ppm, $B(0) = 4,099.2026$ million hectares, and $V(0) = 49.658288$ million vehicles.

To test the validity of the model, R-squared values are employed [31]. The R-squared values for real data and model predictions of human population, human economic activities, atmospheric CO_2 concentration, forest biomass, and vehicle production are 0.955471914, 0.94694, 0.981052, 0.9535782, and 0.9275, respectively. These values indicate a strong correlation between the real data and the model predictions. The real and model projections of the variables N, H, C, B and V are shown in Fig. 1. It is evident from the figure that there is a close alignment between the model projections and the actual data, which ensures the validity of the model.

Furthermore, we applied statistical metrics to assess the performance of our model, including the Root Mean Squared Error Normalized (RMSEN) and the Nash-Sutcliffe Efficiency index (NSE). RMSEN, as it approaches zero, serves as a positive indicator of the model's effectiveness. To classify model performance, we follow the criteria established in previous research [33,34], where RMSEN is considered excellent if it is less than or equal to 10%, good between 10% and 20%, reasonable between 20% and 30%, and poor if it exceeds 30%.

On the other hand, the coefficient of efficiency (NSE) quantifies the overall deviation between real and predicted values from the actual data (R_i) and its mean (R). The NSE value can range from $-\infty$ to $+1$, with higher values indicating efficient model predictions. By using Formula (26), we calculated NSE to be 0.9343, suggesting efficient model predictions. Additionally, employing Formula (25), we obtained an RMSEN value of 2.6027%, further supporting the assessment of excellent model predictions.

In Equation (25), R_i represents the actual data value, R denotes the mean of actual data points, S_i represents the model's predicted data points, and n signifies the number of observations.

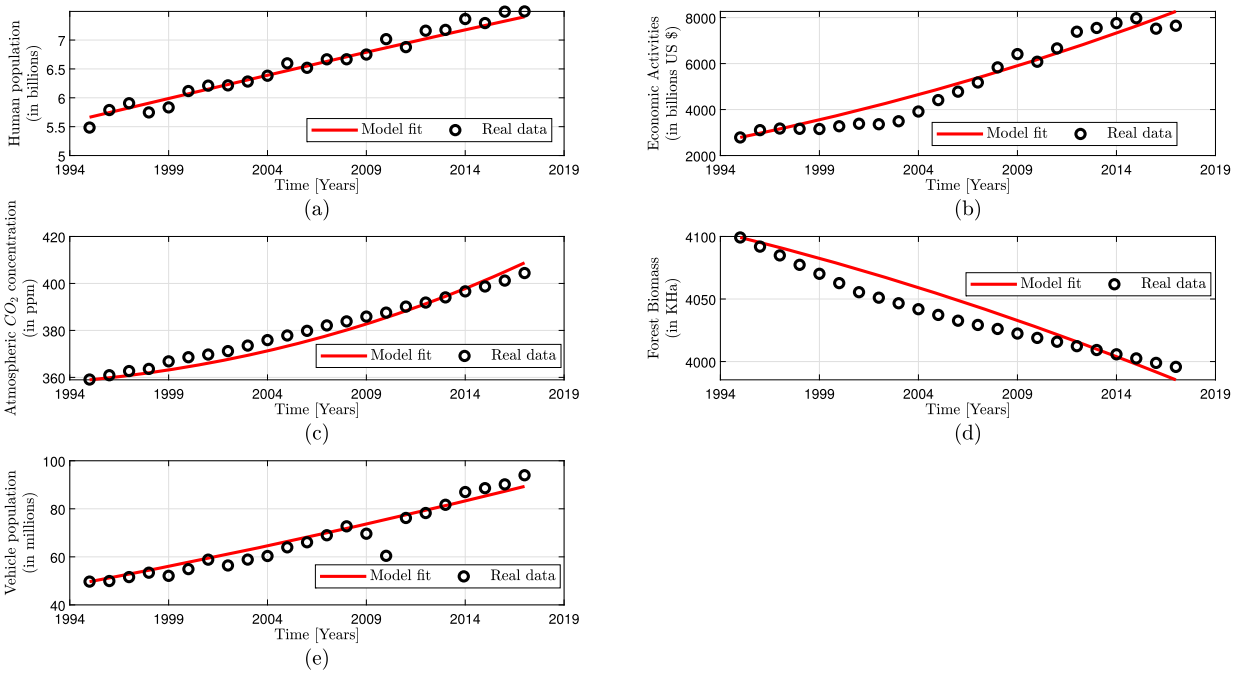

Fig. 1. Comparison between model fit and real data of (a) Human population, (b) Economic activities, (c) Atmospheric CO_2 concentration, (d) Forest biomass and (e) Vehicle population. The curve illustrates that there is a close alignment between the model solution and the observed data.

Table 2
Estimated model parameters, 95% confidence intervals, initial guess for parameters and their respective source.

Parameter	Baseline	Source	Interval	Estimated
r	0.026	[31]	[0.022645 0.03378]	0.0285245
α	0.000001	[32]	$[7.3998\times10^{-7}\ 1.2967\times10^{-6}]$	0.0000010551
τ	3.94	Assumed	-	3.94
s	0.035	[19]	[0.01752 0.04611]	0.03374
γ	4.9337×10^{-7}	Assumed	$[1.6407\times10^{-8}\ 2.3026\times10^{-8}]$	1.3657×10^{-8}
σ	0.000576	Assumed	[0.0005178 0.00079]	0.0007897
η	6.67×10^{-7}	Assumed	-	6.67×10^{-7}
π	0.016	[32]	[0.009668 0.0221]	0.016232
θ	0.0523	Assumed	[0.000909 0.001425]	0.0012025
β	0.0729	Assumed	[0.27216 0.30054]	0.27534
ψ	0.26×10^{-3}	Assumed	[0.0003480.0004031]	0.38874×10^{-3}
ρ	4.8×10^{-9}	[32]	$[0.8662\times10^{-6}\ 1.461\times10^{-6}]$	3.86657×10^{-7}
ξ	1.0676×10^{-6}	Assumed	$[8.374\times10^{-6}\ 1.05005\times10^{-5}]$	1.50623×10^{-5}
ω	0.001	Assumed	[0.00072517 0.0013074]	0.00094457

$$RMSEN = 100\times\frac{1}{R}\sqrt{\frac{1}{n}\times\sum_{i=1}^{n}(R_i - S_i)^2} \tag{25}$$

$$NSE = 1 - \frac{\sum_{i=1}^{n}\left(R_i - S_i\right)^2}{\sum_{i=1}^{n}\left(R_i - R\right)^2} \tag{26}$$

In addition, to assess the robustness of model fitting, we computed 95% confidence intervals for the parameter estimates, as presented in Table 2. These confidence intervals strongly suggest a 95% likelihood of containing the true parameter value. To construct these confidence intervals, we employed a bootstrapping resampling technique with 1000 different data samples, each of the same size as the original datasets. We then re-estimated model parameters for each data sample. It is worth noting that the true parameter value is encompassed within the calculated intervals in 95% of the cases. The narrow width of these confidence intervals underscores the reliability of the model's parameter estimates. Notably, the value of r falls within the range specified by [31], providing further support for the credibility of the parameter estimation. The combination of these tests confirms the robustness of the model's parameter estimates, affirming its suitability for predictive purposes.

4.2. Parameter sensitivity analysis

In order to grasp the impact of model parameters on the system output, we conducted a global sensitivity analysis (GSA) employing partial ranking correlation coefficient (PRCC) which use Latin Hypercube sampling Monte Carlo simulation (LHS). This approach allows us to assess how changes in individual parameters can influence the overall model output [35,36]. A positive PRCC indicate a positive correlation between model parameters and its output. Meaning that increase in the magnitude of a model parameter value will lead to a significant increase in the model output, and a decrease in parameter value will result to a reduced model output. Conversely, a negative PRCC suggest an inverse relationship between parameter value and the model predictions [37]. Observing Fig. 2(a), it is evident that atmospheric CO_2 concentration is significantly accelerated by the growth rate of the vehicle population, denoted as β, and the emission rate of human activities, represented by σ, which is heavily influenced by β and the intrinsic growth rate of the human population, depicted in Fig. 2(c). Furthermore, the PRCC values for the mortality rate due to adverse impacts of enhanced atmospheric CO_2 (α), γ, σ, and β suggest that an increase in these values will lead to a decline in the human population. Conversely, increasing values of r, π, ω, θ, and ψ are associated with an increase in the human population, as illustrated in Fig. 2(b). Also, high values of human population intrinsic growth rate r, lead to the increased demand for mobility as depicted in Fig. 2(d) as the result deforestation will be increased as shown in Fig. 2(e). Analyzing the PRCC values, we pinpointed several highly influential parameters, notably the growth rate of the vehicle population (β), the CO_2 emission rate from human activities (σ) which is triggered by vehicle population, and the intrinsic growth rate of the human population (r). These findings strongly indicate that taking measures to reduce atmospheric CO_2 concentration and addressing the adverse effects of increased emissions from transportation could be pivotal in promoting environmentally friendly transportation practices.

4.3. Numerical simulation

To validate feasibility of the model analysis, we utilized MATLAB R2021a and Maple 2015 software. The chosen set of parameters from Table 2 satisfied the condition (8) for the existence of interior equilibrium point E^*. The eigenvalues of the Jacobian matrix corresponding to the equilibrium point E^* were calculated to be $-3.160388, -0.224952, -0.87302, -5.85509 \times 10^{-7}$, and -0.15062, all of which are negative. This indicates that the equilibrium point E^* is locally asymptotically stable and the condition (24) for global stability of E^* is satisfied for estimated parameter values. Furthermore, the solution trajectories of the model (6) are plotted in Fig. 3 with different starting values. It can be observed that all trajectories initiated inside the region Ω converge towards the interior equilibrium point E^*. This demonstrates the nonlinear stability behavior of the point E^* in the $N(t) - V(t) - B(t)$ and $N(t) - B(t) - C(t)$ space, as depicted in Fig. 3.

To investigate the impact of increased vehicular CO_2 emissions on the human population, we manipulated the most sensitive parameter, denoted as β (as depicted in Fig. 2(c)), within our model. As shown in Fig. 4(a), doubling the vehicle population growth rate has a noticeable effect on the temporal evolution of atmospheric CO_2 concentration, illustrated in Fig. 4(b). The data clearly shows that as the vehicle population increases, atmospheric CO_2 concentration rises.

When we assess the implications of this heightened transportation activity, with the vehicle population growth rate doubled (as shown in Fig. 4(a)), it stimulates economic growth, increasing it from 64,670.4 billion US dollars to 1,071,774 billion US dollars (as depicted in Fig. 4(c)). Simultaneously, atmospheric CO_2 levels increase from 1578 ppm to 2299.83 ppm (as seen in Fig. 4(b)). This results in a reduction in the human population, declining from 10.5255 billion to 10.3976 billion after 100 years as shown in Fig. 4(d).

5. Conclusion

At present time, the control of CO_2 emission along with fulfilling demand for mobility of both humans, goods and services is one of the important issues from ecological and environmental perspectives. The rapid increase in population influences the growth of atmospheric CO_2 concentration and hence climate change issues become more pronounced. In the present study, we have proposed and analyzed a non-linear mathematical model for vehicular CO_2 emission in relation to human population, economic activities, forest biomass and vehicle population.

The proposed model is useful to predict the long-term impact of vehicle CO_2 emission on atmospheric CO_2 evolution and human population. To verify the validity of a model, the model is simulated by using the real world datasets and model parameters fitted to these datasets. All conditions for existence and stability of the interior equilibrium point are satisfied by the estimated data. Numerical simulation shows that an increase in the vehicle CO_2 emission rate results to an increase of atmospheric CO_2 concentration as a result human population depletes due to adverse impact of enhanced atmospheric CO_2 concentration.

In addition, we conducted a global sensitivity analysis of the model parameters using PRCC. The analysis revealed that the atmospheric CO_2 concentration is significantly influenced by the growth rate of the vehicle population (β), the intrinsic human population growth rate (r), and the CO_2 emissions from human activities triggered by the growth in the vehicle population. Furthermore, we identified a connection between the decline in human population and the adverse impacts of increased atmospheric CO_2 concentration and the CO_2 emission rate from human activities (σ). These findings underscore the importance of considering sustainable transportation practices to mitigate the negative impacts on human population caused by an elevated atmospheric CO_2 concentration.

Therefore, to reduce the atmospheric CO_2 concentration, efforts to lower the emission from vehicles are advised so as to attain the seventh and thirteenth Sustainable Development Goals (SDG'S). The present study is not merely confined to consider the impact

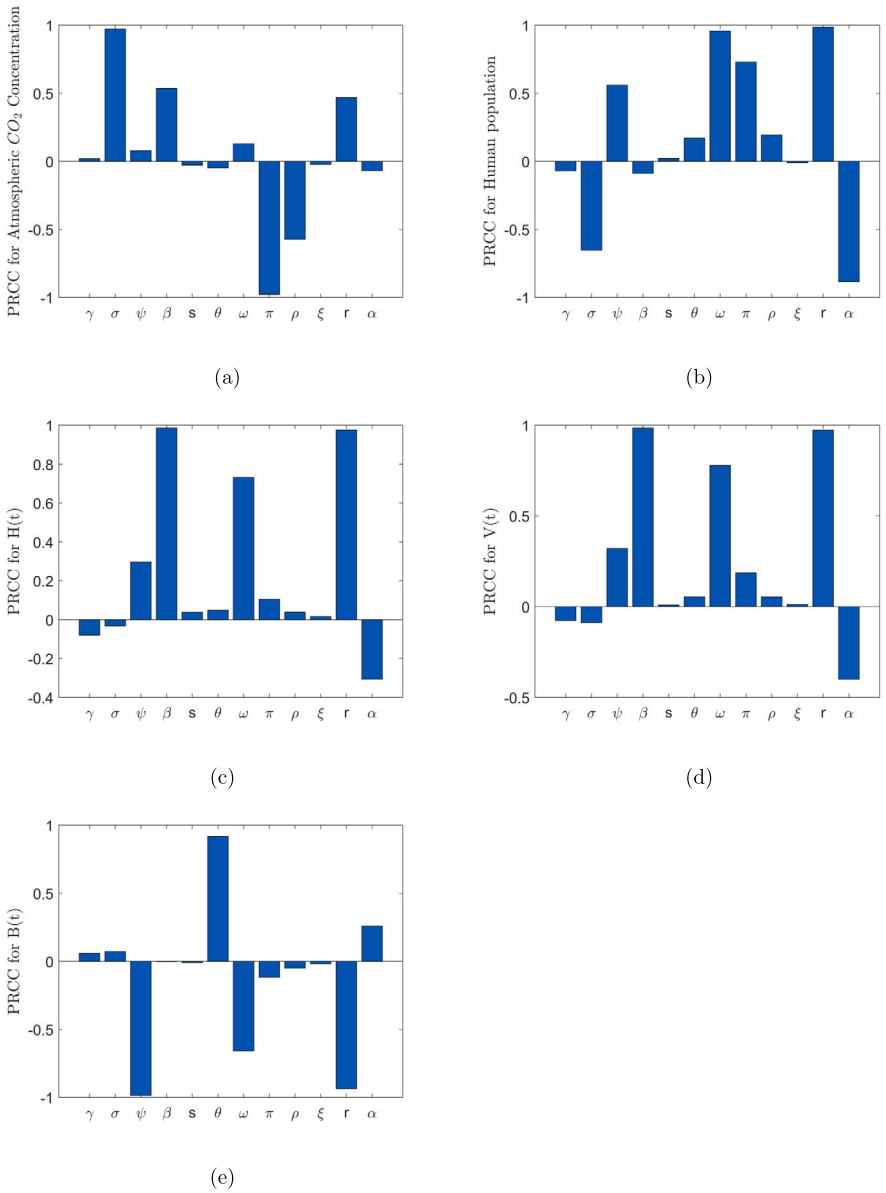

Fig. 2. Sensitivity analysis of model dynamics conducted through 1000 simulations using Latin Hypercube Sampling (LHS). Partial Rank Correlation Coefficients (PRCCs) with respect to atmospheric CO_2 concentration, human population, human economic activities, vehicle population, and forest biomass are presented in graphs (a), (b), (c), (d), and (e), respectively.

of electric vehicles, shared mobility facilities such as Bus rapid Transit (BRT) and alternative transportation modes on atmospheric CO_2 dynamics. Instead, it offers a foundational structure for predicting the long-term effects of atmospheric CO_2 concentration in relation to transport related emissions and human population with the help of analytical results. This will enable the development of strategies to alleviate the potential negative consequences of increased levels of carbon dioxide (CO_2). The present study can be extended to include the impact of electric vehicles, shared mobility facilities and alternative transportation modes on atmospheric CO_2 dynamics.

CRediT authorship contribution statement

Pita Donald: Writing – review & editing, Writing – original draft, Validation, Methodology, Investigation, Formal analysis, Conceptualization. **Maranya Mayengo:** Writing – review & editing, Writing – original draft, Supervision, Methodology, Investigation, Formal analysis, Conceptualization. **Aristide G. Lambura:** Writing – review & editing, Writing – original draft, Supervision, Methodology, Formal analysis, Conceptualization.

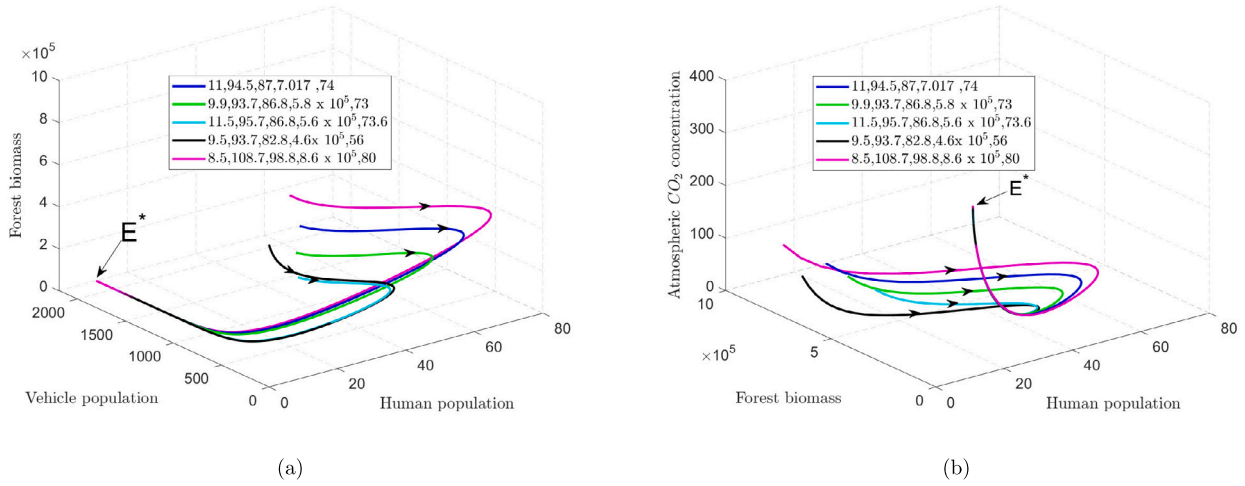

Fig. 3. Graphical representation for global stability of an interior equilibrium point E^* in $N-V-B$ Fig. 3 (a) and $N-V-C$ Fig. 3 (b). All solution trajectories with different initial start are attracted to the interior equilibrium point E^*.

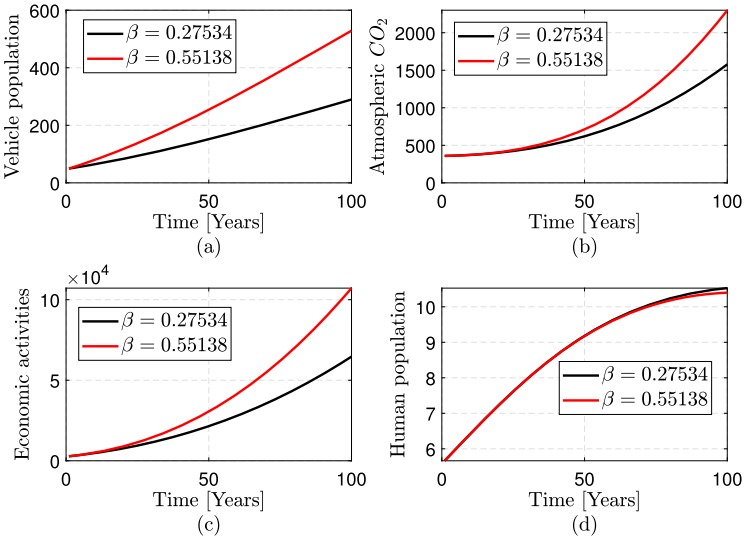

Fig. 4. Impact of increased transportation activities on time evolution of atmospheric CO_2 Fig. 4(b), economic activities Fig. 4(c), and human population Fig. 4(d). As vehicle population is doubled, results to an increase in the atmospheric CO_2 concentration and decline in human population.

Declaration of competing interest

The authors assert that they do not have any identifiable financial conflicts of interest or personal relationships that could have potentially influenced the findings presented in this paper.

Data availability

The data that support the findings of this study are available at the repositories listed below.

1. World Bank Open Data (WBOD). population, total. https://data.worldbank.org/indicator/SP.POP.TOTL, Accessed: 2022-12-16
2. World Bank Open data (WBOD): GDP (current US dollar), World Bank national accounts data, and OECD National Accounts data files https://data.worldbank.org/indicator/NY.GDP.MKTP.CD, Accessed: 2022-12-16
3. Food and Agriculture Organization (FAO), electronic files and web site, https://data.worldbank.org/indicator/AG.LND.FRST.K2., Accessed: 2022-12-16
4. National Oceanic and Atmospheric Administration (NOAA). Trends in Atmospheric Carbon Dioxide, Mauna Loa CO2 annual mean data. https://gml.noaa.gov/ccgg/trends/data.html, Accessed: 2022-12-16 & Our Word in Data (OWD), CO2 emissions https://ourworldindata.org/co2-emissions

5. Beureau of Transportation Statistics (BTS). World Motor Vehicle Production. https://www.bts.gov/content/world-motor-vehicle-production-selected-countries, Accessed: 2022-12-16

Funding

No any fund received in accomplishing this study.

Acknowledgements

Authors are thankful to the handling editor and reviewer for their useful suggestions which improved the quality of this paper. Also, we gratefully acknowledge The Nelson Mandela African Institution of Science and Technology (NM-AIST) and National Institute of Transport (NIT).

Appendix A. Proof of Theorem 4

To analyze the global stability of the interior equilibrium E^*, we use Lyapunov stability theory. Consider the following scalar valued positive definite function

$$\begin{aligned} U &= \left(N - N^* - N^* \ln \frac{N^*}{N}\right) + \frac{1}{2}k_1 (H - H^*)^2 + \frac{1}{2}k_2 (C - C^*)^2 \\ &\quad + \frac{1}{2}k_3 \left(B - B^* - B^* \ln \frac{B^*}{B}\right) + \frac{1}{2}k_4 (V - V^*)^2 \end{aligned} \tag{A.1}$$

Where k_1, k_2, k_3 and k_4 are suitable positive constants to be determined later.
Differentiating U with respect to t;

$$\frac{dU}{dt} = \frac{\partial U}{\partial N}\left(\frac{dN}{dt}\right) + \frac{\partial U}{\partial H}\left(\frac{dH}{dt}\right) + \frac{\partial U}{\partial C}\left(\frac{dC}{dt}\right) + \frac{\partial U}{\partial B}\left(\frac{dB}{dt}\right) + \frac{\partial U}{\partial V}\left(\frac{dV}{dt}\right) \tag{A.2}$$

Performing algebraic operations we get the following;

$$\begin{aligned} \frac{dU}{dt} &= -\frac{r}{L}(N - N^*)^2 - \eta k_1 (H - H^*)^2 - k_2 (\rho K + \pi)(C - C^*)^2 - \frac{\theta k_3}{K}(B - B^*)^2 \\ &\quad -\xi k_4 (V - V^*)^2 + \alpha (C - C^*)(N - N^*) + \psi \left(\omega - k_3\right)(B - B^*)(N - N^*) \\ &\quad +s k_1 (H - H^*)(N - N^*) + \tau k_1 (V - V^*)(H - H^*) + \gamma k_2 (V - V^*)(C - C^*) \\ &\quad +\sigma k_2 (H - H^*)(C - C^*) + \beta k_4 (N - N^*)(V - V^*) \end{aligned} \tag{A.3}$$

Choosing $k_3 = \omega$ we have the following;

$$\begin{aligned} \frac{dU}{dt} &= -\frac{r}{L}(N - N^*)^2 - \eta k_1 (H - H^*)^2 - k_2 (\rho K + \pi)(C - C^*)^2 - \frac{\theta k_3}{K}(B - B^*)^2 \\ &\quad -\xi k_4 (V - V^*)^2 + \alpha (C - C^*)(N - N^*) + s k_1 (H - H^*)(N - N^*) \\ &\quad +\tau k_1 (V - V^*)(H - H^*) + \gamma k_2 (V - V^*)(C - C^*) \\ &\quad +\sigma k_2 (H - H^*)(C - C^*) + \beta k_4 (N - N^*)(V - V^*) \end{aligned} \tag{A.4}$$

Choosing $k_1 = \frac{\eta r}{s^2 L}$, $k_2 = 1$, $k_3 = \omega$ and $k_4 = \frac{\xi r}{\beta^2 L}$, $\frac{dU}{dt}$ is negative definite under conditions (24), hence the Theorem (4) is proved.

Appendix B. Proof of Lemma 1

From the fourth equation of model system (6), we have

$$\frac{dB}{dt} \leq \theta B \left(1 - \frac{B}{K}\right). \tag{B.1}$$

By comparing the above differential inequality with the differential equation

$$\frac{dB}{dt} = \theta B \left(1 - \frac{B}{K}\right). \tag{B.2}$$

and using comparison theorem, we have

$$B(t) \leq \frac{K}{1 + \left(\frac{K}{B(0)} - 1\right) e^{-\theta t}}. \tag{B.3}$$

Let $\epsilon > 0$ be given. Then $\exists_{t_0 \geq 0}$ such that

$$B(t) \leq K + \epsilon \qquad \forall_{t \geq t_0}. \tag{B.4}$$

This gives

$$\limsup_{t\to\infty} B(t) \le B_m. \tag{B.5}$$

Now from the first equation of the model system (6), we have

$$\frac{dN}{dt} \le (r + \omega\psi(K+\epsilon))\, N - \frac{rN^2}{L} \qquad \forall_{t\ge t_0}. \tag{B.6}$$

Using the same argument as previously, $\exists_{t_1\ge t_0}$ such that

$$N(t) \le (r + \omega\psi(K+\epsilon))\, \frac{L}{r} + \epsilon = N_\epsilon \quad , \quad \forall_{t\ge t_1\ge t_0}. \tag{B.7}$$

Hence

$$\limsup_{t\to\infty} N(t) \le N_m. \tag{B.8}$$

From second equation in the model system (6), we get

$$\frac{dH}{dt} \le sN_\epsilon - \eta H \qquad \forall_{t\ge t_1}. \tag{B.9}$$

Then we have

$$H(t) \le \frac{sN_\epsilon}{\eta} + \epsilon = H_\epsilon \quad , \quad \forall_{t\ge t_2\ge t_1}. \tag{B.10}$$

Hence

$$\limsup_{t\to\infty} H(t) \le H_m. \tag{B.11}$$

From third equation of the model system (6)

$$\frac{dC}{dt} \le C_0 + \sigma H\epsilon - \rho(K+\epsilon)C - \pi C \qquad \forall_{t\ge t_2}. \tag{B.12}$$

$\exists_{t_3\ge t_2}$ such that

$$C(t) \le \frac{C_0 + \sigma H_\epsilon}{\rho(K+\epsilon)+\pi} + \epsilon = C_\epsilon \qquad \forall_{t\ge t_3\ge t_2}. \tag{B.13}$$

Hence

$$\limsup_{t\to\infty} C(t) \le C_m. \tag{B.14}$$

Similarly, it can be easily shown that $\limsup_{t\to\infty} V(t) \le \frac{\beta N_m}{\xi}$. Thus, the Lemma 1 is proved.

Appendix C. Supplementary material

Supplementary material related to this article can be found online at https://doi.org/10.1016/j.heliyon.2024.e23976.

References

[1] J.-C. Yeh, C.-H. Liao, Impact of population and economic growth on carbon emissions in Taiwan using an analytic tool STIRPAT, Sustain. Environ. Res. 27 (1) (2017) 41–48, https://doi.org/10.1016/j.serj.2016.10.001.

[2] A. Majewska, U. Gierałtowska, Impact of economic affluence on CO2 emissions in CEE countries, Energies 15 (1) (2022) 322, https://doi.org/10.3390/en15010322.

[3] J. Hussain, A. Khan, K. Zhou, The impact of natural resource depletion on energy use and CO2 emission in Belt Road Initiative countries: a cross-country analysis, Energy 199 (2020) 117409, https://doi.org/10.1016/j.energy.2020.117409.

[4] S. Pal, I. Ghosh, Dynamics of a coupled socio-environmental model: an application to global CO2 emissions, Ecol. Model. 478 (2023) 110279, https://doi.org/10.1016/j.ecolmodel.2023.110279.

[5] A. Mohammadi, A.A. Burhan, R. Mangal, Impact of population and economic growth on CO2 emission (case of Afghanistan), J. Emerg. Technol. Innov. Res. (2020).

[6] M. Appiah, F. Li, B. Korankye, Modeling the linkages among CO2 emission, energy consumption, and industrialization in sub-Saharan African (SSA) countries, Environ. Sci. Pollut. Res. 28 (29) (2021) 38506–38521, https://doi.org/10.1007/s11356-021-12412-z.

[7] T. Boden, G. Marland, R. Andres, Global, regional, and national fossil-fuel co2 emissions, 1751 - 2006 (published 2009), https://doi.org/10.3334/CDIAC/00001, 2009.

[8] W.F. Lamb, T. Wiedmann, J. Pongratz, R. Andrew, M. Crippa, J.G.J. Olivier, D. Wiedenhofer, G. Mattioli, A.A. Khourdajie, J. House, S. Pachauri, M. Figueroa, Y. Saheb, R. Slade, K. Hubacek, L. Sun, S.K. Ribeiro, S. Khennas, S. de la Rue du Can, L. Chapungu, S.J. Davis, I. Bashmakov, H. Dai, S. Dhakal, X. Tan, Y. Geng, B. Gu, J. Minx, A review of trends and drivers of greenhouse gas emissions by sector from 1990 to 2018, Environ. Res. Lett. 16 (7) (2021) 073005, https://doi.org/10.1088/1748-9326/abee4e.

[9] Y. Li, J. Shang, C. Zhang, W. Zhang, L. Niu, L. Wang, H. Zhang, The role of freshwater eutrophication in greenhouse gas emissions: a review, Sci. Total Environ. 768 (2021) 144582, https://doi.org/10.1016/j.scitotenv.2020.144582.
[10] X. Zhao, A. Mahendra, N. Godfrey, H. Dalkmann, P. Rode, G. Floater, Unlocking the power of urban transport systems for better growth and a better climate, in: The New Climate Economy, 2016.
[11] V.N. Pedreira, M.L. Brito, L.C.L. dos Santos, G. Simonelli, Modeling of Brazilian carbon dioxide emissions: a review, Braz. Arch. Biol. Technol. 65 (2022), https://doi.org/10.1590/1678-4324-2022210594.
[12] IEA, CO2 emissions from fuel combustion 2019 edition, IEA CO2 emissions from fuel combustion database, Available at http://wds.iea.org, 2019.
[13] D. Helbing, D. Brockmann, T. Chadefaux, K. Donnay, U. Blanke, O. Woolley-Meza, M. Moussaid, A. Johansson, J. Krause, S. Schutte, M. Perc, Saving human lives: what complexity science and information systems can contribute, J. Stat. Phys. 158 (3) (2014) 735–781, https://doi.org/10.1007/s10955-014-1024-9.
[14] A.K. Misra, K. Lata, A mathematical model to achieve sustainable forest management, Int. J. Model. Simul. Sci. Comput. 06 (04) (2015) 1550040, https://doi.org/10.1142/s1793962315500403.
[15] S. Devi, N. Gupta, Dynamics of carbon dioxide gas: effects of varying capability of plants to absorb CO2, Nat. Resour. Model. 32 (1) (2018) e12174, https://doi.org/10.1111/nrm.12174.
[16] A.K. Misra, M. Verma, A mathematical model to study the dynamics of carbon dioxide gas in the atmosphere, Appl. Math. Comput. 219 (16) (2013) 8595–8609, https://doi.org/10.1016/j.amc.2013.02.058.
[17] M. Verma, A.K. Verma, A.K. Misra, Mathematical modeling and optimal control of carbon dioxide emissions from energy sector, Environ. Dev. Sustain. 23 (9) (2021) 13919–13944, https://doi.org/10.1007/s10668-021-01245-y.
[18] A.K. Misra, M. Verma, E. Venturino, Modeling the control of atmospheric carbon dioxide through reforestation: effect of time delay, Model. Earth Syst. Environ. 1 (3) (Sep. 2015), https://doi.org/10.1007/s40808-015-0028-z.
[19] M.A.L. Caetano, D.F.M. Gherardi, T. Yoneyama, Optimal resource management control for CO2 emission and reduction of the greenhouse effect, Ecol. Model. 213 (1) (2008) 119–126, https://doi.org/10.1016/j.ecolmodel.2007.11.014.
[20] A.J. McMichael, R.E. Woodruff, S. Hales, Climate change and human health: present and future risks, Lancet 367 (9513) (2006) 859–869, https://doi.org/10.1016/s0140-6736(06)68079-3.
[21] S.A. Roosa, A.G. Jhaveri, Carbon reduction technologies, in: Energy Management Handbook, Publishers, River, 2020, pp. 561–581.
[22] H.I. Freedman, J.W.-H. So, Global stability and persistence of simple food chains, Math. Biosci. 76 (1) (1985) 69–86, https://doi.org/10.1016/0025-5564(85)90047-1.
[23] WBOD, Population, total [dataset]: https://data.worldbank.org/indicator/SP.POP.TOTL, 2018. (Accessed 16 December 2022).
[24] D.M. Etheridge, L.P. Steele, R.L. Langenfelds, R.J. Francey, J.-M. Barnola, V.I. Morgan, Natural and anthropogenic changes in atmospheric CO2 over the last 1000 years from air in Antarctic ice and firn, J. Geophys. Res., Atmos. 101 (D2) (1996) 4115–4128, https://doi.org/10.1029/95jd03410.
[25] H. Ritchie, M. Roser, P. Rosado, CO2 and greenhouse gas emissions, in: Our World in Data, 2020.
[26] NOAA, Trends in atmospheric carbon dioxide, mauna Loa co2 annual mean data [dataset], https://gml.noaa.gov/ccgg/trends/data.html, 2020. (Accessed 16 December 2022).
[27] FAO, Forest area (sq. km), food and agriculture organization, electronic files and web site [dataset], https://data.worldbank.org/indicator/AG.LND.FRST.K2, 2020. (Accessed 16 December 2022).
[28] BTS, World motor vehicle production [dataset], https://www.bts.gov/content/world-motor-vehicle-production-selected-countries, 2019. (Accessed 16 December 2022).
[29] WBOD, Gdp (current us dollar), world bank national accounts data, and oecd national accounts data files [dataset], https://data.worldbank.org/indicator/NY.GDP.MKTP.CD, 2019. (Accessed 16 December 2022).
[30] F. Gao, L. Han, Implementing the Nelder-Mead simplex algorithm with adaptive parameters, Comput. Optim. Appl. 51 (1) (2010) 259–277, https://doi.org/10.1007/s10589-010-9329-3.
[31] M. Verma, A.K. Verma, Effect of plantation of genetically modified trees on the control of atmospheric carbon dioxide: a modeling study, Nat. Resour. Model. 34 (2) (Feb. 2021), https://doi.org/10.1111/nrm.12300.
[32] M. Verma, A.K. Misra, Optimal control of anthropogenic carbon dioxide emissions through technological options: a modeling study, Comput. Appl. Math. 37 (1) (2016) 605–626, https://doi.org/10.1007/s40314-016-0364-2.
[33] R.V. Ferreira, R.L.M. Tavares, S.F. d. Medeiros, A.G.d. Silva, J.F.d. Silva Júnior, Carbon stock and organic fractions in soil under monoculture and Sorghum bicolor–Urochloa ruziziensis intercropping systems, Bragantia 79 (2020) 425–433.
[34] H. Léonidas, T. Toru, N. Fidel, C.R. Athanase, M. Athanase, Comparative analysis of monocropping and mixed cropping systems on selected soil properties, soil organic carbon stocks, and simulated maize yields in drought-hotspot regions of Rwanda, Heliyon (2023).
[35] T. Azizi, R. Mugabi, Global sensitivity analysis in physiological systems, Appl. Math. 11 (03) (2020) 119–136, https://doi.org/10.4236/am.2020.113011.
[36] S. Bidah, O. Zakary, M. Rachik, Stability and global sensitivity analysis for an agree-disagree model: partial rank correlation coefficient and Latin hypercube sampling methods, Int. J. Differ. Equ. 2020 (2020) 1–14, https://doi.org/10.1155/2020/5051248.
[37] I.M. Fanuel, S. Mirau, D. Kajunguri, F. Moyo, Conservation of forest biomass and forest–dependent wildlife population: uncertainty quantification of the model parameters, Heliyon 9 (6) (2023).